

# Cumulants of net-strangeness multiplicity distributions at energies available at the BNL Relativistic Heavy Ion Collider

Changfeng Li,<sup>1</sup> Deeptak Biswas,<sup>2</sup> and Nihar Ranjan Sahoo<sup>1,3,4</sup>

<sup>1</sup>*Institute of Frontier and Interdisciplinary Science,  
Shandong University, Qingdao, Shandong, 266237, China*

<sup>2</sup>*The Institute of Mathematical Sciences, a CI of Homi Bhabha National Institute, Chennai, 600113, India*

<sup>3</sup>*Key Laboratory of Particle Physics and Particle Irradiation,  
Shandong University, Qingdao, Shandong, 266237, China*

<sup>4</sup>*National Institute of Science Education and Research, HBNI, Jatni 752050, India*

(Dated: June 12, 2023)

The higher-order cumulants of net-proton number, net-charge, and net-strangeness multiplicity distributions are widely studied to search for the quantum-chromodynamics critical point and extract the chemical freeze-out parameters in heavy-ion collisions. In this context, the event-by-event fluctuations of the net-strangeness multiplicity distributions play important roles in extracting the chemical freeze-out parameter in the strangeness sector. Due to having difficulties in detecting all strange hadrons event by event, the kaon ( $K$ ) and lambda ( $\Lambda$ ) particles serve as a proxy for the strangeness-related observables in heavy-ion collisions. We have studied the net- $K$ , net- $\Lambda$ , and net- $(K+\Lambda)$  multiplicity distributions and calculated their different order of cumulants using the ultrarelativistic quantum molecular dynamics model and hadron resonance gas calculation. To adequately account for the net-strangeness cumulants, it has been found that the inclusion of resonance decay contributions in  $K$  and  $\Lambda$  is necessary.

## I. INTRODUCTION

A deconfined phase of quantum chromodynamics (QCD) matter—known as the quark-gluon plasma—is created by colliding heavy ions at the BNL Relativistic Heavy-Ion Collider (RHIC) and the CERN Large Hadron Collider (LHC). The main goal of the RHIC Beam Energy Scan (BES) program is to search for the QCD critical point and gauge the QCD phase diagram in temperature ( $T$ ) and baryon chemical potential ( $\mu_B$ ) plane. In BES phase-I, the STAR experiment reported several measurements on the higher-order cumulants of net-charge [1], net-proton number [2–4], net-kaon [5], and net- $\Lambda$  [6] multiplicity distributions as well. These cumulants are associated with their respective conserved charge susceptibilities, and hence these are related to thermodynamic quantities, like  $T$  and  $\mu_B$ , in heavy-ion collisions.

The net-proton number cumulant measurements are proposed as the proxy of net-baryon number susceptibility; hence, it is used to search for the location of the QCD critical point [7] in heavy-ion collision. References [2–4] have reported several net-proton cumulant measurements. In addition, one can extract the chemical freeze-out (CFO) temperature and  $\mu_B$  in the heavy-ion collisions with the help of these cumulants [8–10].

On the other hand, the cumulants of net-kaon and net- $\Lambda$  multiplicity distribution act as a proxy for the strangeness and help to extract the CFO parameters from the strangeness sector, especially strangeness chemical potential ( $\mu_S$ ) and the respective temperature. The standard practice is to extract these parameters using the strange hadron yields [11, 12] and also the higher order cumulants of net-strangeness multiplicity distributions. The inclusion of different resonances in the thermal

model fit influences the CFO parameter [13]. The freeze-out temperature increases with the inclusion of heavier hadrons [11, 14]. Furthermore, the strange meson freezes out earlier than lighter hadrons at the highest RHIC energy, as studied in Refs.[15, 16]. Hence it is important to know the other strange baryons' freeze-out temperature and their chemical potential in heavy-ion collisions.

In this paper, we study the cumulants of net-kaon, net- $\Lambda$ , and net-(kaon+ $\Lambda$ ) multiplicity distributions using the ultrarelativistic quantum molecular dynamics (UrQMD) model and the centrality variation for the STAR energies. To estimate the degree of thermalization, we have compared the most central results from UrQMD with the hadron resonance gas (HRG) calculation. These results would set a baseline for the ongoing measurements in the STAR experiment. The CFO parameters extracted from the thermal model fit of the particle yields are used in the HRG calculations to match the net-kaon and net- $\Lambda$  higher-order cumulant data from the STAR results [12]. A one-to-one comparison between UrQMD and HRG results for the net-(kaon+ $\Lambda$ ) elucidates the necessity to consider the contribution of the feed-down from the decay of higher mass resonance into the thermal model to explain the net-strangeness observable at RHIC energies.

This paper is organized as follows. In Sec. II A, the definition of net-(kaon+ $\Lambda$ ) and their cumulants are introduced. A brief introduction of the UrQMD model and HRG calculation are mentioned in Secs. II B and II C, respectively. The net-kaon, net- $\Lambda$ , and net-(kaon+ $\Lambda$ ) cumulants and their ratios are discussed in Sec. III A. The comparison between the UrQMD and HRG calculations for the net- $K$  and net- $\Lambda$  multiplicity distributions is discussed in Sec. III B. The strangeness production and resonance decay effects are discussed in Sec. III C. Finally, we summarize our studies and outline the STAR mea-

measurements as an outlook in Sec. IV.

## II. OBSERVABLES AND MODELS

### A. Cumulants of Net-(kaon+ $\Lambda$ ) multiplicity distributions

We define the number of net-(kaon+ $\Lambda$ ) [in short net-( $K+\Lambda$ )] as

$$N_{K+\Lambda} = (N_{K^+} + N_{\bar{\Lambda}}) - (N_{K^-} + N_{\Lambda}). \quad (1)$$

Here,  $N_x$  is the number of  $x$  particle in an event within a given phase space window, where  $x$  is  $K^+(u\bar{s})$ ,  $K^-(\bar{u}s)$ ,  $\Lambda(uds)$ , or  $\bar{\Lambda}(\bar{u}\bar{d}\bar{s})$ . Here, the  $(N_{K^+} + N_{\bar{\Lambda}})$  and  $(N_{K^-} + N_{\Lambda})$  represents the total positive and negative strangeness quantum numbers in an event, respectively. In heavy-ion collisions, the initial strangeness is zero. Note here that the STAR net-kaon and net- $\Lambda$  publications are reported with  $(N_{K^+} - N_{K^-})$  in net-kaon [5] and  $(N_{\Lambda} - N_{\bar{\Lambda}})$  in net- $\Lambda$  measurements [6], respectively.

The  $\langle N \rangle$  is the ensemble average of multiplicity in a given centrality class. The deviation of  $N$  from its mean  $\langle N \rangle$  is defined as  $\delta N = N - \langle N \rangle$ . The  $n$ th order of diagonal cumulants ( $C_n$ ) can be defined as

$$C_1 = \langle N \rangle, \quad (2)$$

$$C_2 = \langle (\delta N)^2 \rangle \quad (3)$$

$$C_3 = \langle (\delta N)^3 \rangle \quad (4)$$

$$C_4 = \langle (\delta N)^4 \rangle - 3\langle (\delta N)^2 \rangle^2 \quad (5)$$

A detailed discussion regarding the cumulant-generating function and relationships between moments, central moments, and cumulants can be found in Ref. [17]. In this paper, we discuss different orders of cumulants and their ratios for the net-( $K+\Lambda$ ), net- $K$ , and net-( $\Lambda$ ) multiplicity distributions. The connection between these cumulants and the thermodynamics susceptibilities is discussed in Sec. II C.

### B. UrQMD model

The UrQMD [18, 19] model is a microscopic transport model. In this space-time evolution model, the propagation, rescattering among hadrons, and string excitation are included, whereas no in-medium modification effects are implemented. Hence, this model is used to study the baseline measurement in heavy-ion collisions for various observables [20, 21].

In the present work, the Au+Au collision events are simulated at  $\sqrt{s_{NN}} = 7.7, 11.5, 19.6, 27, 39, 62.4$ , and 200 GeV with minimum-bias configuration (impact parameter,  $b = 0$  to 14 fm). The different particles with their particle data group particle identification in an event

are analyzed using the same phase space window similar to the STAR experiment. The centrality selections are performed based on the charged particle multiplicity distribution at the midrapidity, following the STAR experiment specifications. The net- $K$ , net- $\Lambda$ , and net-( $K+\Lambda$ ) multiplicity distributions are calculated within  $0.4 < p_T < 1.6$  GeV/ $c$  and rapidity window  $|y| < 0.5$ . The cumulants and their ratios are calculated as mentioned in Sec. II A.

### C. HRG calculation

The ideal HRG model considers an ensemble of non-interacting hadrons and their resonances. The logarithm of the partition function can be written as

$$\ln Z^{\text{id}} = \sum_i \ln Z_i^{\text{id}}, \quad (6)$$

where the sum runs over all the hadrons and resonances; the ‘id’ stands for the ideal gas consideration. The Boltzmann approximation provides a reasonable baseline for the massive hadrons and resonances (except  $\pi$ ) along the chemical freeze-out boundary [22]. In this work, the particle species under consideration ( $K, \Lambda$ ) have much higher masses than the freeze-out temperature and  $m_i - \mu_i \gg T$  for the respective freeze-out parametrization. Within this consideration, we can approximate the partition functions in the Boltzmann limit [23]. With such assumption [22],

$$\ln Z_i^{\text{id}} = \pm \frac{V g_i}{2\pi^2} \int_0^\infty p^2 dp e^{-(E_i - \mu_i)/T} \quad (7)$$

where  $V$ ,  $T$ , and  $g_i$  are the system volume, temperature, and degeneracy factor of the  $i$ th hadron.  $E_i = \sqrt{p^2 + m_i^2}$  is the single particle energy.  $\mu_i = B_i \mu_B + S_i \mu_S + Q_i \mu_Q$  is the chemical potential, where  $B_i, S_i$ , and  $Q_i$  are, respectively, the baryon number, strangeness, and charge of the particle. The  $\mu_B, \mu_S$ , and  $\mu_Q$  are the baryon, strangeness, and charge chemical potentials, respectively.

With the Boltzmann approximation, the pressure of a single hadron species  $i$  is defined as [22, 24]

$$P_i^{\text{id}} = \frac{T}{V} \ln Z_i^{\text{id}} = \pm \frac{g_i T}{2\pi^2} \int_0^\infty p^2 dp e^{-(E_i - \mu_i)/T}$$

The  $n$ th order susceptibility is defined as

$$\chi_x^n = \frac{1}{VT^3} \frac{\partial^n (\ln Z)}{\partial \left(\frac{\mu_x}{T}\right)^n} \quad (8)$$

where  $\mu_x$  is the chemical potential for conserved charge  $x$ . The derivatives of the logarithm of the grand canonical partition function ( $Z$ ) with respect to the chemical potential define susceptibilities. These susceptibilities are related to the event-by-event measured cumulants of net-charge, net-baryon, and net-strangeness multiplicity distributions. For our present purpose  $x = S$  (strangeness).

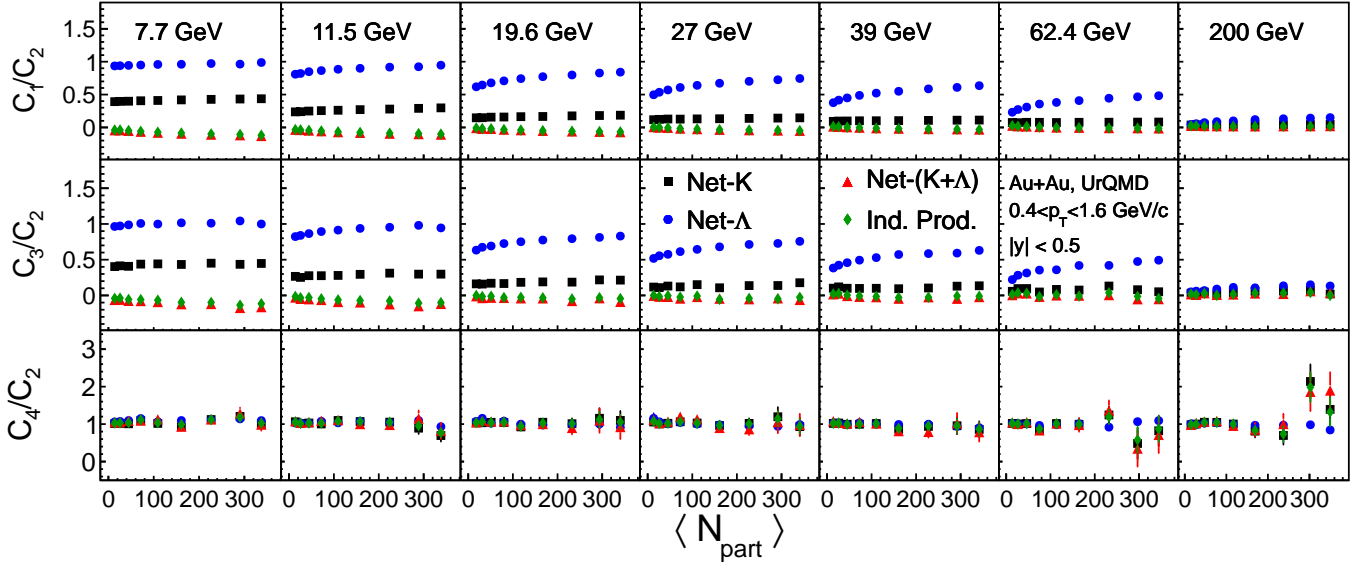


FIG. 1. The cumulants ratios of net- $K$  (box), net- $\Lambda$  (circle), net- $(K + \Lambda)$  (triangle), and independent particle production for net- $(K + \Lambda)$  (diamond) are shown at  $\sqrt{s_{NN}}=7.7-200$  GeV calculated within the same acceptance. The vertical bars are statistical errors.

With the Boltzmann limit in Eq.(7), the  $n$ th order susceptibility can be expressed as,

$$\chi_x^n = \sum_i \frac{g_i x_i^n}{2\pi^2 T^3} \int_0^\infty p^2 dp e^{-(E_i - \mu_i)/T}. \quad (9)$$

This form simplifies the representation of cumulants, making the multiplicity distribution similar to a Poisson distribution [23]. This simplification is due to the fact that the derivative of the exponential function is also exponential and the analytical form is independent of the order of derivative  $n$ . In Boltzmann limit, the relationship between different cumulants becomes straightforward with  $C_1 = C_3$  and  $C_2 = C_4$ . Experimental observations at RHIC energies, as reported by the STAR experiment, confirm this Boltzmann approximation by considering the Poisson distributions in the net- $K$  and net- $\Lambda$  cumulants measurements [5, 6].

#### D. Connection with experimental observable

The event-by-event net-charge multiplicity distributions are measured in heavy-ion experiments within a finite acceptance. The cumulants ( $C_n$ ) discussed in Sec. II A are related to the different order of susceptibilities by the following relation:

$$VT^3 \chi_x^n = C_n. \quad (10)$$

The ratios of these cumulants are taken to cancel the volume term in the above expression. The mean ( $M_q$ ), variance ( $\sigma_q^2$ ), skewness ( $S_q$ ), and kurtosis ( $\kappa_q$ ) are also

related with different cumulants as follows:

$$\sigma_q^2/M_q = C_2/C_1 = \chi_q^2/\chi_q^1 \quad (11)$$

$$S_q \sigma_q = C_3/C_2 = \chi_q^3/\chi_q^2 \quad (12)$$

$$\kappa_q \sigma_q^2 = C_4/C_2 = \chi_q^4/\chi_q^2 \quad (13)$$

### III. RESULTS AND DISCUSSION

#### A. Cumulants of Net- $K$ , net- $\Lambda$ , and net- $(K+\Lambda)$ in UrQMD

The  $K^-/K^+$  yield ratio increases with collision energy and approaches to unity at higher collision energy [11] due to the interplay between associated production ( $NN \rightarrow KYN$ ,  $\pi N \rightarrow KY$ ) and pair production ( $NN \rightarrow NNK^+K^-$ ). The  $\bar{\Lambda}/\Lambda$  yield ratio also shows the same trend as a function of collision energy [25]. Recent net- $K$  [5] and net- $\Lambda$  [6] measurements show that the  $C_1$  of these multiplicity distributions are positive and increase with centrality and also collision energy. In this paper, we calculate the cumulant ratios of net- $K$ , net- $\Lambda$ , and net- $(K+\Lambda)$  multiplicity distributions for seven collision energies using the UrQMD model.

Figure 1 shows the three cumulant ratios  $C_1/C_2$ ,  $C_3/C_2$ , and  $C_4/C_2$  for the net- $K$ , net- $\Lambda$ , and net- $(K+\Lambda)$  multiplicity distributions from  $\sqrt{s_{NN}}=7.7$  to 200 GeV. The  $C_1/C_2$  for net-kaon and net- $\Lambda$  is always positive as a function of centrality. Contrarily, this is negative up to  $\sqrt{s_{NN}}=39$  GeV for net- $(K+\Lambda)$ . Negative  $C_1$  is responsible for the negative value of this ratio. A similar trend is observed in the case of  $C_3/C_2$ . The negative  $C_1$  and  $C_3$  are responsible for making these ratios negative

for net- $(K+\Lambda)$ . The  $C_4/C_2$  is almost the same for three cases at all energies and remains around unity.

On the contrary, the mean value ( $C_1$ ) of net- $(K+\Lambda)$  is negative at lower energy, whereas it becomes positive at  $\sqrt{s_{NN}}=200$  GeV in Au+Au collisions in UrQMD. Here, we reiterate the combined quantity,  $N_{K+\Lambda} = (N_{K^+} + N_{\bar{\Lambda}}) - (N_{K^-} + N_{\Lambda})$ . We can understand this trend as the following. More baryons are produced at the lower collision energy due to the higher baryon deposition. The  $\Lambda$  particle, being the lightest strange baryon, dominates the net- $(K+\Lambda)$  and gives rise to this negative value. This negative trend decreases as the collision energy increases and particle-to-antiparticle yields become similar. This implies more negative net-strangeness number (more  $s$  quarks) is observed at lower collision energies than at the top collision energy.

Furthermore, to study the correlation contribution between  $(N_{K^+} + N_{\bar{\Lambda}})$  and  $(N_{K^-} + N_{\Lambda})$  to net- $(K+\Lambda)$  distribution, we calculate the following expression for the independent particle production:

$$C_n^{K+\Lambda} = C_n(N_{K^+} + N_{\bar{\Lambda}}) + (-1)^n C_n(N_{K^-} + N_{\Lambda}). \quad (14)$$

It should be noted that the expression mentioned above is built on the basis of Eq. (1). After examining the comparison between the assumption of independent particle production and cumulant computed from the sample of net- $(K+\Lambda)$  distributions in the UrQMD model, there seems to be a negligible difference. However, it is essential to incorporate experimental data to study these correlations in the BES energies.

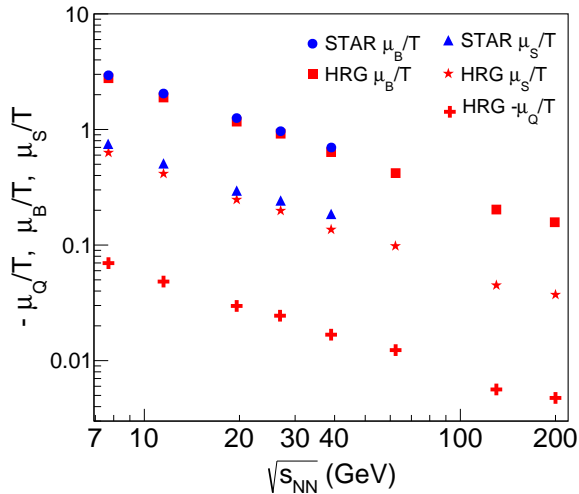


FIG. 2. The  $\mu_B/T$ ,  $\mu_S/T$  and  $-\mu_Q/T$  as a function of  $\sqrt{s_{NN}}$ . The red color markers are the input parameters used in HRG calculation to match the STAR net-kaon [5] and net- $\Lambda$  [6] data as shown in Fig. 3 and 4. The blue markers are the thermal model fit from the STAR data [12].

## B. Comparison with HRG

A comparison between the UrQMD results and HRG calculation is important to understand the underlying hadronic scattering contribution to these observables and set a baseline for heavy-ion collision experiments. To study the degree of thermalization, we calculated the HRG estimations at the chemical freeze-out boundary. Reference [26] has shown that various cumulants (up to third order) of different species can describe the susceptibilities calculated in the HRG using a grand canonical ensemble above certain colliding energy, which restricts the applicability of the HRG model to the fireball created in low-energy heavy-ion collisions.

In Fig. 2, we present the variation of  $\mu_B/T$ ,  $\mu_S/T$ , and  $\mu_Q/T$  with collision energy ( $\sqrt{s_{NN}}$ ), which are evaluated by fitting the yield data with the thermal model assuming a grand-canonical ensemble. The particle yields, including  $\pi$ ,  $K$ ,  $p$ ,  $\Lambda$ ,  $\Xi$ , and  $\Omega$ , are used to estimate these parameters [27–29]. While the strangeness and baryon chemical potential values are consistent with those reported by the STAR collaboration [11, 12], there are no reported values for  $\mu_Q$ . We have included these parameters along with the available ones for a comprehensive analysis, as they serve as input parameters for HRG calculations. We must emphasize that these parameter values result from fitting the yield and are included here for completeness.

Using these parameters, we will initially compare the ratios of cumulants for individual species. Previous studies [30, 31] have shown that the decay feed-down does not significantly affect the ratios of cumulants up to the third order for individual species.

Figure 3 shows the  $M/\sigma^2$  and  $S\sigma$  of net- $K$  as a function of collision energy ( $\sqrt{s_{NN}}$ ). The HRG calculations are carried out using the same acceptance cuts as employed in the STAR measurements [6]. The HRG calculation and UrQMD results exhibit a good agreement with experimental data for both these ratios.

Figure 4 shows the  $M/\sigma^2$  and  $S\sigma$  of net- $\Lambda$  as a function of collision energy ( $\sqrt{s_{NN}}$ ). The HRG calculations well explain the data both for the  $M/\sigma^2$  and  $S\sigma$  results. The UrQMD estimations have a large deviation from the experimental data for net- $\Lambda$ , which mainly comes from the disagreement in the values of  $C_2$  [6]. Note here that no decay contributions are included in these HRG calculations.

The comparison between the UrQMD model and HRG calculations shows that the net- $K$  results are comparable and also match the data. The net- $\Lambda$  results have an apparent difference between the UrQMD and HRG calculations. The UrQMD result for net- $\Lambda$  deviates from the data at all energies. The higher mass resonances decay channels are included in the UrQMD events. This difference in the net- $\Lambda$   $M/\sigma^2$  and  $S\sigma$  results from the UrQMD could be due to the difference in the  $\Lambda$ , higher resonance (anti)particle production yields in UrQMD, and the RHIC energies [19].

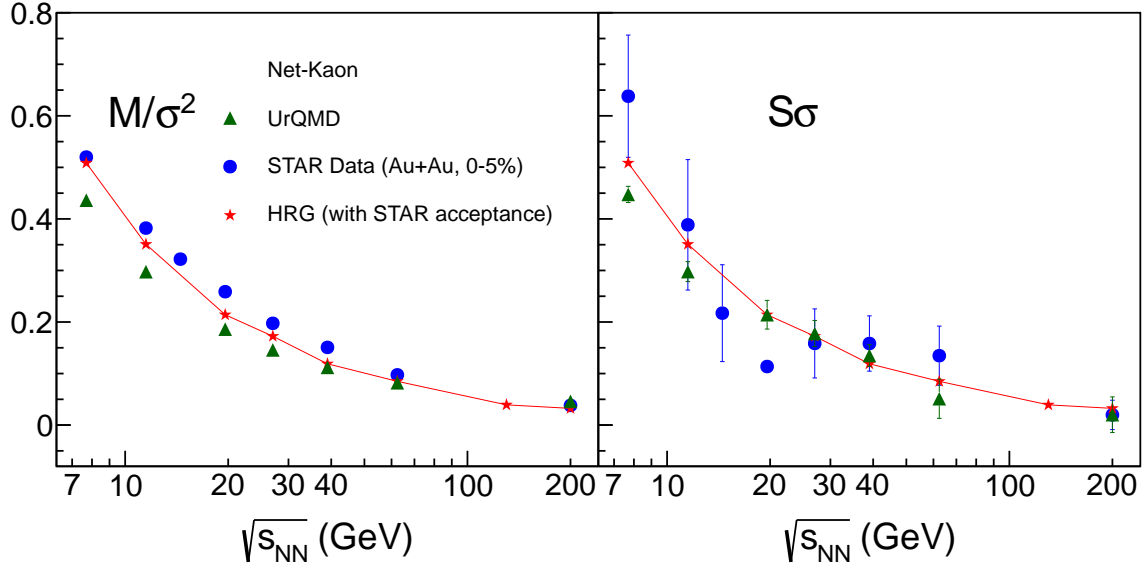


FIG. 3. The  $M/\sigma^2$  ( $C_1/C_2$ ) (left panel) and  $S\sigma$  ( $C_3/C_2$ ) (right panel) of net- $K$  as a function  $\sqrt{s_{NN}}$ . The circles, star markers, and triangles represent the STAR data, HRG calculations (done with the same kinematic cuts as the data), and the UrQMD model calculations, respectively. Net-kaon data are from Ref. [5].

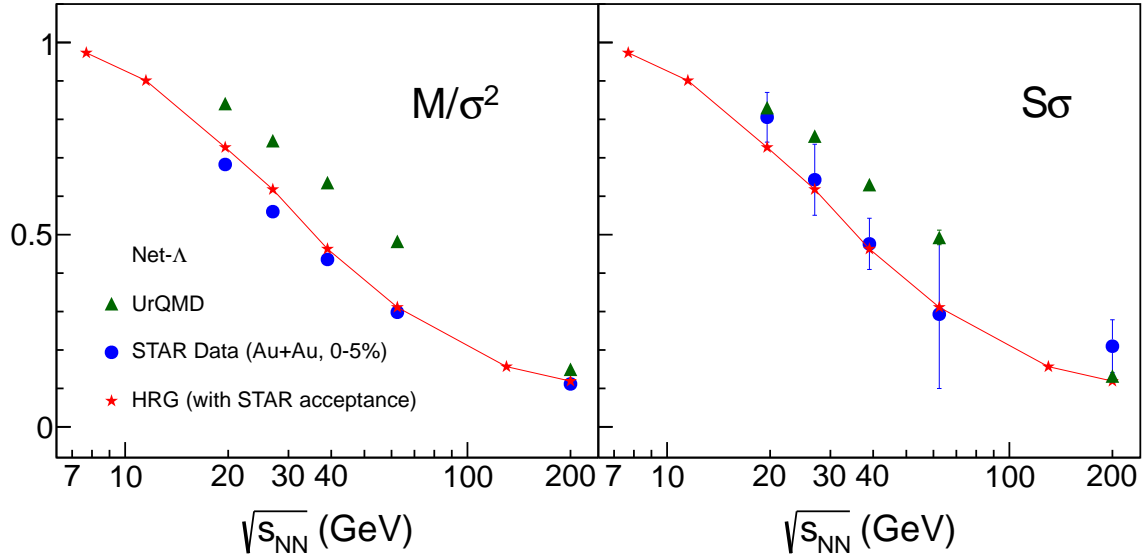


FIG. 4. The  $M/\sigma^2$  ( $C_1/C_2$ ) (left panel) and  $S\sigma$  ( $C_3/C_2$ ) (right panel) of net- $\Lambda$  as a function  $\sqrt{s_{NN}}$ . The circles, star markers, and triangles represent the STAR data, HRG calculations (done with the same kinematic cuts as the data), and the UrQMD model calculations, respectively. Net- $\Lambda$  data are from Ref. [6].

Here, it is worth noting that the quantitative similarity between the ratios  $C_1/C_2$  ( $M/\sigma^2$ ) and  $C_3/C_2$  ( $S\sigma$ ) establishes the applicability of the Boltzmann approximation in the context of heavy-ion collisions, i.e.,  $C_3 = C_1$ . The good agreement among the HRG results with the Boltzmann statistics and the experimental data validates the Poisson limit of the particle distribution. Any deviation from this Poisson limit is due to the additional underlying physics present in the data. With a general agreement

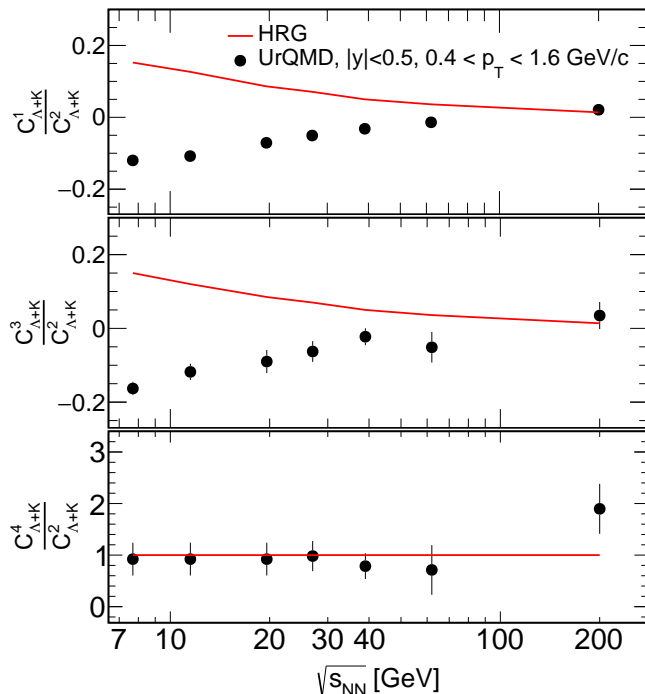


FIG. 5. The energy dependence of  $C_1/C_2$ ,  $C_3/C_2$ , and  $C_4/C_2$  for 0–5 % centrality for the UrQMD model (circles) and the HRG calculation (red line).

among UrQMD results, STAR data, and HRG calculations, it would be interesting to compare results for the net- $(K+\Lambda)$  multiplicity distribution. As no experimental data are available yet for this combination, we have compared the UrQMD results with those from the HRG model. In the framework of the ideal HRG model, the cumulants of net- $(K+\Lambda)$  are just the addition of the cumulants of the net-kaon and net- $\Lambda$ . Within the Poisson distribution approximation, this simple addition assumes a Skellam distribution, where  $C_1 = C_3$ ,  $C_2 = C_4$ . The  $C_1$  is the difference between the mean in the case of cumulants of net quantities. This simplified picture thus provides a trivial baseline for the cumulant study.

In Fig. 5, the energy dependence of the net- $(K+\Lambda)$   $C_1/C_2$ ,  $C_3/C_2$ , and  $C_4/C_2$  for 0–5% central Au+Au collisions in the UrQMD model and HRG calculations are compared. The  $C_1/C_2$  and  $C_3/C_2$  show an opposite trend at lower collision energy between the UrQMD and the thermal model predictions. The HRG calculations have been performed with the chemical freeze-out

parametrization from Refs. [27–29]. This disagreement is prominent at lower collision energy. This difference arises from higher mass resonance decay in the UrQMD model, whereas no such decay feed-down is included in the HRG calculations. A detailed discussion on the importance of higher mass resonance decay contributions can be found in Sec. III C. The  $C_4/C_2$  of HRG calculation is unity at all energies and consistent with the UrQMD models. It shows that  $C_4/C_2$  is less sensitive to the resonance contributions.

### C. Strangeness production in HRG

In heavy-ion collisions, the strange particles' yields contain the contribution from the decay feed-down of higher mass resonances [11, 12]. In the thermal model, it is important to include all higher mass resonance decay channels to capture the bulk description of the chemical freeze-out surface properly. Inclusion of these decays for higher order susceptibility calculations needs to consider the probabilistic nature of decay channels through their branching fractions [30, 32–34]. Including these decay products in the yield, calculations are trivial as those are the first cumulant (mean). The (anti-) $\Lambda(1115)$  has the contributions from the higher mass strange baryons, e.g.,  $\Sigma(1385)$ ,  $\Lambda(1405)$ ,  $\Lambda(1520)$ , and other heavy resonances. Kaons (493) have contributions mostly from the higher mass meson resonances like  $K^*(892)$ ,  $K(1270)$ ,  $\phi(1020)$ , etc. However, for kaons, the inclusion of all resonances becomes complex as many resonances decay into both  $K^+$  and  $K^-$ . In this work, we have not included any decay channels from the higher resonances for the susceptibility calculation in the HRG. To quantify the relevance of decay from the higher mass resonances, we have plotted the ratio of the mean value of the net- $(K+\Lambda)$  with that of the total in Fig. 6. The model calculations are performed following the freeze-out parameters from Refs. [27, 28, 35]. These parameters were extracted with the mean value of yields and successfully explained the hadronic yield ratios. By including decays from higher mass resonances, the model agrees with the data, whereas the ratio increases with decreasing beam energy if we exclude the decay contribution. Hence, for a reasonable estimate of the parametrization and to explain the data, it is necessary to include the higher mass resonance decay in the calculation of the net-strangeness observable.

Although the strangeness neutrality demands the net-strangeness to be zero in the total system and distributed among the final particle species in the whole phase space. Here, we investigate only the charged kaon(493) and  $\Lambda(1115)$ . With increasing  $\mu_B$  at lower collision energies, strange baryons dominate, and the strangeness gets distributed mainly among the hyperons. The  $\Lambda$  being the lightest one contributes the most significant part. The decay from higher mass resonances increases the yield of  $\Lambda$  and produces a net negative strangeness at lower collision energies. With only the primary abundance, the net



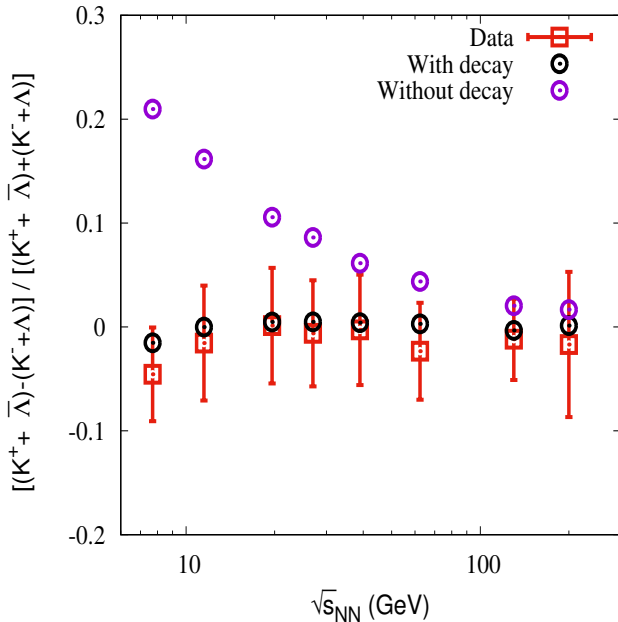


FIG. 6. The ratio of the net to the total charged kaon and  $\Lambda$  multiplicity as a function of  $\sqrt{s_{NN}}$ . The black (with decay) and purple (without decay) circles represent the HRG calculations. The data (box) are from Ref.[12]

strangeness remains positive in our observable, as the lightest kaons dominate the sum and deliver a positive strangeness. Such behaviors can be seen in the UrQMD model calculation as it includes all resonance decays in an event, as discussed in Sec. III B.

#### IV. SUMMARY AND OUTLOOK

In heavy-ion collision experiments, observables related to net- $K$  and net- $\Lambda$  act as a proxy for the strangeness. Although the individual results for net- $K$  and net- $\Lambda$  are available from STAR BES, results for the combined study for the net- $(K+\Lambda)$  are yet to be performed. In this work, we have studied the cumulants of net- $K$ , net- $\Lambda$ , and net- $(K+\Lambda)$  multiplicity distributions for the RHIC BES energy range using the UrQMD model. These studies serve as a baseline for the cumulant measurement of the net- $(K+\Lambda)$  multiplicity distributions.

In UrQMD, the  $C_1/C_2$  and  $C_3/C_2$  of net- $(K+\Lambda)$  are negative at lower energies and become positive at higher collision energies within the given acceptance window mentioned in this paper. At lower  $\sqrt{s_{NN}}$ , the

finite baryon density favors the dominance of hyperons over strange mesons, which produces this negative strangeness. This effect diminishes as the collision energy increases and the kaon becomes more abundant than the hyperons. On the contrary, the higher-order cumulant  $C_4/C_2$  has no significant variation between net- $K$ , net- $\Lambda$ , and net- $(K+\Lambda)$  multiplicity distributions.

As a benchmark, we have compared our UrQMD calculations of various cumulants with available STAR data of net- $K$  and net- $\Lambda$  for the most central collision, where a good agreement is apparent. Furthermore, we have compared the UrQMD results with the HRG calculation to study the thermalization contribution to these observables. The HRG calculations have been performed at the standard chemical freeze-out parametrization. Although there is good agreement among data, UrQMD calculations and model(HRG) predictions for the individual net- $K$  and net- $\Lambda$ , differences among UrQMD results and HRG for cumulant ratios of net- $(K+\Lambda)$  are apparent.

It seems that the difference between the decay feed-down of higher mass resonances is responsible for the difference between UrQMD and HRG. The decay consideration is necessary to explain the available experimental data, which is responsible for a negative  $C_1$  and  $C_3$  at lower collision energies.

This net- $(K+\Lambda)$  cumulant measurements along with that of net- $K$  and net- $\Lambda$  multiplicity distributions can provide necessary information on the strangeness in heavy-ion collisions at RHIC energies, and will act as a benchmark for future experiments. It is important to compare these calculations from the UrQMD and HRG with the STAR ongoing measurements. The STAR's BES-II data with lower collision energies in the fixed target experiment could provide important information about the strangeness production and their event-by-event fluctuations in heavy-ion collisions. The proper treatment of the decay feed-down into kaon and  $\Lambda$  would facilitate the extraction of the chemical freeze-out parameters from the strangeness sector.

#### ACKNOWLEDGEMENT

We would like to thank Bedangadas Mohanty, Tapan Nayak, Sayantan Sharma, Qinghua Xu, Zhangbu Xu, and Li Yi for their fruitful discussion and comments on this work. N.R.S. would like to acknowledge IMSc, Chennai, for hospitality during his visit where this work was started. N.R.S. is supported by the Fundamental Research Funds of Shandong University and the National Natural Science Foundation of China, Grant No. 12050410235.

[1] L. Adamczyk *et al.* [STAR], Phys. Rev. Lett. **113**, 092301 (2014) doi:10.1103/PhysRevLett.113.092301

[arXiv:1402.1558 [nucl-ex]].

- [2] L. Adamczyk *et al.* [STAR], Phys. Rev. Lett. **112**, 032302 (2014) doi:10.1103/PhysRevLett.112.032302 [arXiv:1309.5681 [nucl-ex]].
- [3] J. Adam *et al.* [STAR], Phys. Rev. Lett. **126**, no.9, 092301 (2021) doi:10.1103/PhysRevLett.126.092301 [arXiv:2001.02852 [nucl-ex]].
- [4] M. S. Abdallah *et al.* [STAR], Phys. Rev. Lett. **128**, no.20, 202303 (2022) doi:10.1103/PhysRevLett.128.202303 [arXiv:2112.00240 [nucl-ex]].
- [5] L. Adamczyk *et al.* [STAR], Phys. Lett. B **785**, 551-560 (2018) doi:10.1016/j.physletb.2018.07.066 [arXiv:1709.00773 [nucl-ex]].
- [6] J. Adam *et al.* [STAR], Phys. Rev. C **102**, no.2, 024903 (2020) doi:10.1103/PhysRevC.102.024903 [arXiv:2001.06419 [nucl-ex]].
- [7] M. A. Stephanov, Prog. Theor. Phys. Suppl. **153**, 139-156 (2004) doi:10.1142/S0217751X05027965 [arXiv:hep-ph/0402115 [hep-ph]].
- [8] A. Bazavov, H. T. Ding, P. Hegde, O. Kaczmarek, F. Karsch, E. Laermann, S. Mukherjee, P. Petreczky, C. Schmidt and D. Smith, *et al.* Phys. Rev. Lett. **109**, 192302 (2012) doi:10.1103/PhysRevLett.109.192302 [arXiv:1208.1220 [hep-lat]].
- [9] S. Gupta, D. Mallick, D. K. Mishra, B. Mohanty and N. Xu, [arXiv:2004.04681 [hep-ph]].
- [10] S. Sharma, Int. J. Mod. Phys. E **30**, no.07, 2130003 (2021) doi:10.1142/S0218301321300034 [arXiv:2103.13641 [hep-lat]].
- [11] L. Adamczyk *et al.* [STAR], Phys. Rev. C **96**, no.4, 044904 (2017) doi:10.1103/PhysRevC.96.044904 [arXiv:1701.07065 [nucl-ex]].
- [12] J. Adam *et al.* [STAR], Phys. Rev. C **102**, no.3, 034909 (2020) doi:10.1103/PhysRevC.102.034909 [arXiv:1906.03732 [nucl-ex]].
- [13] P. Alba, V. M. Sarti, J. Noronha-Hostler, P. Parotto, I. Portillo-Vazquez, C. Ratti and J. M. Stafford, Phys. Rev. C **101**, no.5, 054905 (2020) doi:10.1103/PhysRevC.101.054905 [arXiv:2002.12395 [hep-ph]].
- [14] S. Mitra, [arXiv:2010.09706 [nucl-th]].
- [15] R. Bellwied, J. Noronha-Hostler, P. Parotto, I. Portillo Vazquez, C. Ratti and J. M. Stafford, Phys. Rev. C **99**, no.3, 034912 (2019) doi:10.1103/PhysRevC.99.034912 [arXiv:1805.00088 [hep-ph]].
- [16] J. Chen, J. Deng, Z. Tang, Z. Xu and L. Yi, Phys. Rev. C **104**, no.3, 034901 (2021) doi:10.1103/PhysRevC.104.034901 [arXiv:2012.02986 [nucl-th]].
- [17] M. Kitazawa and X. Luo, Phys. Rev. C **96**, no.2, 024910 (2017) doi:10.1103/PhysRevC.96.024910 [arXiv:1704.04909 [nucl-th]].
- [18] M. Bleicher, E. Zabrodin, C. Spieles, S. A. Bass, C. Ernst, S. Soff, L. Bravina, M. Belkacem, H. Weber and H. Stoecker, *et al.* J. Phys. G **25**, 1859-1896 (1999) doi:10.1088/0954-3899/25/9/308 [arXiv:hep-ph/9909407 [hep-ph]].
- [19] S. A. Bass, M. Belkacem, M. Bleicher, M. Brandstetter, L. Bravina, C. Ernst, L. Gerland, M. Hofmann, S. Hofmann and J. Konopka, *et al.* Prog. Part. Nucl. Phys. **41**, 255-369 (1998) doi:10.1016/S0146-6410(98)00058-1 [arXiv:nucl-th/9803035 [nucl-th]].
- [20] X. Luo, B. Mohanty and N. Xu, Nucl. Phys. A **931**, 808-813 (2014) doi:10.1016/j.nuclphysa.2014.08.105 [arXiv:1408.0495 [nucl-ex]].
- [21] A. Chatterjee, S. Chatterjee, T. K. Nayak and N. R. Sahoo, J. Phys. G **43**, no.12, 125103 (2016) doi:10.1088/0954-3899/43/12/125103 [arXiv:1606.09573 [nucl-ex]].
- [22] S. Wheaton and J. Cleymans, Comput. Phys. Commun. **180**, 84-106 (2009) doi:10.1016/j.cpc.2008.08.001 [arXiv:hep-ph/0407174 [hep-ph]].
- [23] M. Kitazawa and M. Asakawa, Phys. Rev. C **86**, 024904 (2012) [erratum: Phys. Rev. C **86**, 069902 (2012)] doi:10.1103/PhysRevC.86.024904 [arXiv:1205.3292 [nucl-th]].
- [24] P. Huovinen and P. Petreczky, Phys. Lett. B **777**, 125-130 (2018) doi:10.1016/j.physletb.2017.12.001 [arXiv:1708.00879 [hep-ph]].
- [25] A. Andronic, P. Braun-Munzinger and J. Stachel, Nucl. Phys. A **772**, 167-199 (2006) doi:10.1016/j.nuclphysa.2006.03.012 [arXiv:nucl-th/0511071 [nucl-th]].
- [26] S. Gupta, D. Mallick, D. K. Mishra, B. Mohanty and N. Xu, Phys. Lett. B **829**, 137021 (2022) doi:10.1016/j.physletb.2022.137021
- [27] D. Biswas, Phys. Rev. C **102**, no.5, 054902 (2020) doi:10.1103/PhysRevC.102.054902 [arXiv:2007.07680 [nucl-th]].
- [28] S. Bhattacharyya, D. Biswas, S. K. Ghosh, R. Ray and P. Singha, Phys. Rev. D **100**, no.5, 054037 (2019) doi:10.1103/PhysRevD.100.054037 [arXiv:1904.00959 [nucl-th]].
- [29] S. Bhattacharyya, D. Biswas, S. K. Ghosh, R. Ray and P. Singha, Phys. Rev. D **101**, no.5, 054002 (2020) doi:10.1103/PhysRevD.101.054002 [arXiv:1911.04828 [hep-ph]].
- [30] D. K. Mishra, P. Garg, P. K. Netrakanti and A. K. Mohanty, Phys. Rev. C **94**, no.1, 014905 (2016) doi:10.1103/PhysRevC.94.014905 [arXiv:1607.01875 [hep-ph]].
- [31] P. Garg, D. K. Mishra, P. K. Netrakanti, B. Mohanty, A. K. Mohanty, B. K. Singh and N. Xu, Phys. Lett. B **726**, 691-696 (2013) doi:10.1016/j.physletb.2013.09.019 [arXiv:1304.7133 [nucl-ex]].
- [32] V. V. Begun, M. I. Gorenstein, M. Hauer, V. P. Konchakovski and O. S. Zozulya, Phys. Rev. C **74**, 044903 (2006) doi:10.1103/PhysRevC.74.044903 [arXiv:nucl-th/0606036 [nucl-th]].
- [33] M. Nahrgang, M. Bluhm, P. Alba, R. Bellwied and C. Ratti, Eur. Phys. J. C **75**, no.12, 573 (2015) doi:10.1140/epjc/s10052-015-3775-0 [arXiv:1402.1238 [hep-ph]].
- [34] H. j. Xu, Phys. Lett. B **765**, 188-192 (2017) doi:10.1016/j.physletb.2016.12.015 [arXiv:1612.06485 [nucl-th]].
- [35] D. Biswas, Adv. High Energy Phys. **2021**, 6611394 (2021) doi:10.1155/2021/6611394 [arXiv:2003.10425 [hep-ph]].